MNRAS **000**, 1–10 (2015) Preprint 26 July 2018 Compiled using MNRAS LATEX style file v3.0

Explaining changing-look AGN with state transition triggered by rapid mass accretion rate drop

Hirofumi Noda[1,2,3⋆] and Chris Done[3]
[1] *Frontier Research Institute for Interdisciplinary Sciences, Tohoku University, 6-3 Aramakiazaaoba, Aoba-ku, Sendai, Miyagi 980-8578, Japan*
[2] *Astronomical Institute, Tohoku University, 6-3 Aramakiazaaoba, Aoba-ku, Sendai, Miyagi 980-8578, Japan*
[3] *Centre for Extragalactic Astronomy, Department of Physics, University of Durham, South Road, Durham DH1 3LE, UK*

Accepted 2018 July 25. Received 2018 July 20; in original form 2018 May 20

ABSTRACT

We model the broadband (optical/UV and X-ray) continuum spectrum of the "changing-look" active galactic nucleus (AGN) Mrk 1018 as it fades from Seyfert 1 to 1.9 in ~ 8 years. The brightest spectrum, with Eddington ratio $L/L_{\rm Edd} \sim 0.08$, has a typical type 1 AGN continuum, with a strong "soft X-ray excess" spanning between the UV and soft X-rays. The dimmest spectrum, at $L/L_{\rm Edd} \sim 0.006$, is very different in shape as well as luminosity, with the soft excess dropping by much more than the hard X-rays. The soft X-ray excess produces most of the ionizing photons, so its dramatic drop leads to the disappearance of the broad line region, driving the "changing-look" phenomena. This spectral hardening appears similar to the soft-to-hard state transition in black hole binaries at $L/L_{\rm Edd} \sim 0.02$, where the inner disc evaporates into an advection dominated accretion flow, while the overall drop in luminosity appears consistent with the Hydrogen ionization disc instability. Nonetheless, both processes happen much faster in Mrk 1018 than predicted by disc theory. We critically examine scaling from galactic binary systems, and show that a major difference is that radiation pressure should be much more important in AGNs, so that the sound speed is much faster than expected from the gas temperature. Including magnetic pressure to stabilize the disc shortens the timescales even further. We suggest that all changing-look AGNs are similarly associated with the state transition at $L/L_{\rm Edd} \sim$ a few percent.

Key words: galaxies: active – galaxies: individual (Mrk 1018) – galaxies: Seyfert – X-rays: galaxies

1 INTRODUCTION

The optical variability of active galactic nuclei (AGNs) is puzzling. The viscous timescale for changing the mass accretion rate onto a supermassive black hole (SMBH) is extremely long for a standard thin disc at radii corresponding to those which produce the optical emission, at least thousands of years for typical AGN parameters. Yet AGNs typically show stochastic optical variability of a factor of a few on timescales of months–years (e.g., Kelly et al. 2009; MacLeod et al. 2010). This flux change could instead be produced from reprocessing of the X-ray emission from a central compact source. An X-ray tail accompanies the disc emission in all AGNs (e.g., Elvis et al. 1994; Lusso & Risaliti 2016) requiring that some of the gravitational power is dissipated in optically thin material rather than in the optically thick, geometrically thin disc. These X-rays vary on rapid timescales, indicating that they come from a compact region around the SMBH, and the fast variable X-ray heating can result in fast optical variability (Clavel et al. 1992). However, while reprocessing can provide an overall explanation of the fast timescales, reverberation studies of the optical continuum imply size scales which are generally a factor of a few larger than the thin disc predictions (e.g., Shappee et al. 2014; Troyer et al. 2016; Noda et al. 2016), and detailed models which use the observed X-ray emission to predict the optical flux do not match well to the observed light curves (e.g., Gardner & Done 2017).

Nonetheless, a factor of a few discrepancy in size scale and/or issues with the detailed shape of the light curve is clearly less problematic than the original factor of $\gtrsim 10^4$ difference in timescale. Hence some form of X-ray reprocessing is the favoured model for the stochastic, small scale (a few tens of percent) optical variability (see e.g., Lawrence 2012). However, this is much more difficult for systems which show larger amplitude variability. Some of these can be due to extrinsic effects, such as obscuration events, where material from the clumpy molecular torus moves into or out of the

⋆ E-mail: hirofumi.noda@astr.tohoku.ac.jp

line of sight (e.g., Elitzur 2012; Gardner & Done 2017), or microlensing (e.g., Lawrence et al. 2016), but clearly there is an intrinsic change in luminosity in systems where the emission lines also respond. In particular, a small subset of AGNs change from type 1 (showing both broad and narrow lines) to type 1.9 (where the broad lines almost disappear) or vice versa, associated with a change by more than a factor 2 in continuum flux ("changing-look" AGN: see e.g., LaMassa et al. 2015 and references therein). Some of these also show more extreme variability associated with the "changing look", where the continuum changes by more than a factor of $\gtrsim 10$ over a timescale of years (e.g., Graham et al. 2017). These objects are rare, but are now being increasingly discovered in large surveys with repeat cadence (e.g., MacLeod et al. 2016).

We focus here on one particularly well studied case of extreme variability associated with a "changing look". The bare (low intrinsic absorption) nucleus Mrk 1018 changed from type 1 to 1.9 around 1980 (Cohen et al. 1986) and from type 1.9 to 1 around 2010 (McElroy et al. 2016). This event is unlikely to be associated with uncovering/covering of the central AGN by a dusty cloud from the torus as the timescale does not correspond to the expected orbital velocity out at torus size scales, nor is there any progressive change in reddening as the source brightens/dims. Instead, for an intrinsic change in UV continuum, the BLR clouds should respond to the changing photo-ionizing flux (LOC: Baldwin et al. 1995; Korista et al. 1997; Korista & Goad 2000), while the NLR stays constant due to the much longer light travel timescales.

The broad lines are most sensitive to the extreme ultraviolet (EUV) part of the spectral energy distribution (SED), and this ionizing flux is mostly unobservable due to galactic absorption. Nonetheless, multiple studies show that the continuum emission turns down below the expected disc emission as the spectrum approaches the Lyman limit at ~ 1000 Å, while it turns up above the extrapolated 2–10 keV X-ray power-law emission in the soft X-ray region. These two spectral breaks point towards each other, and can be fitted by a Comptonization spectrum dominating the ionizing flux in the FUV region. The parameters of this Comptonization region are remarkably similar across multiple AGNs, indicating that there is ubiquitous warm ($kT_{\rm e} \sim 0.2$ keV), optically thick material ($\tau \sim 10$–20: e.g., Czerny et al. 2003; Gierliński & Done 2004; Mehdipour et al. 2011; Noda et al. 2011; Noda et al. 2013; Matt et al. 2014; Petrucci et al. 2017; Porquet et al. 2018) as well as an inner hard X-ray corona which is hot ($kT_{\rm e} \sim 50$–100 keV) and optically thin ($\tau \sim 1$). Thus to track the BLR ionizing flux, we need broad band, simultaneous UV and X-ray datasets which can determine the warm and hot Comptonization components as well as any standard disc emission.

The decline of Mrk 1018 from 2008 was fairly well monitored with both optical/UV and X-ray telescopes on *Swift* and *XMM-Newton* (McElroy et al. 2016; Husemann et al. 2016). Hence we can use these data to model the change in soft X-ray excess and hard X-ray emission during the large drop in continuum as the source changed from type 1.0 to 1.9 over an 8 year period.

2 OBSERVATIONS AND DATA REDUCTION

We analyze the archival datasets of Mrk 1018 derived by the EPIC-PN and OM onboard *XMM-Newton*, and by the XRT and UVOT onboard *Swift*. We perform the following data reductions to the individual satellite datasets.

XMM-Newton: The source was observed on 2008 Aug 7 (obsid of 0554920301), hereafter 2008 Aug. We reprocess the PN and OM datasets using `epchain` and `omichain` in `SAS-16.0.0`, respectively. We exclude PN events when the 10–12 keV background count rate is more than 0.35 cnt s^{-1}. The PN source spectrum is extracted from a $40''$-radius circle region centered at the AGN, while the PN background spectrum is from a $1'$-radius circle region off the AGN. The PN response matrix and auxiliary response file are prepared by the `rmfgen` and `arfgen` in `SAS-16.0.0`, respectively. The U, UVW1, and UVW2 spectra are created via `om2pha` using count rates obtained by `omdetect` in the sequence of `omichain` and the response files distributed by the *XMM-Newton* Science Operations Centre.

Swift: The source was observed on 2008 Jun 11 (obsid: 00035776001), 2013 Mar 1 and Jun 7–8, (obsid: 00049654001 and 00049654002), and 2016 Feb 11 and Feb 16 (obsid: 00080898001 and 00080898002). To extract X-ray spectral files including background files, response matrixes and ancillary response files, we use the automated pipeline of the UK *Swift* Science Data Center (Evans et al. 2007, 2009). In the spectral extractions, we request to co-add the two datasets (00049654001, 00049654002) in 2013, and the two (00080898001, 00080898002) in 2016 to get better signal-to-noise, and select events with grade 0–12. These procedures provide three *Swift*/XRT spectra, and hereafter we call them the X-ray spectra in 2008 Jun, 2013 and 2016. We extract the V, B, U, UVW1, UVM2, and the UVW2 count rates from datasets with obsid 00035776001, 00049654001 and 00080898001 to make optical–UV spectra in 2008 Jun, 2013, and 2016, respectively. The commands of `uvotimsum` and `uvot2pha` in `heasoft-6.20` are used to merge multiple extensions, and to convert count rates into XSPEC readable files. The source region is a $5''$-radius circle centered at the AGN while the background is taken from a $50''$-radius circle off the AGN, which includes no other bright sources. We use the response files of the UVOT bands distributed by the UK *Swift* Science Data Center.

By the `grppha` command in `heasoft-6.20`, each X-ray spectrum is binned so that a bin includes at least 20 photons to appropriately employ χ^2 statistics in spectral fits. After the binning, an energy range up to ~ 10 keV is noticed in the *XMM-Newton*/EPIC-PN spectrum, while we ignore the *Swift*/XRT spectra in an energy range of $\gtrsim 6$ keV where the number of photons is less than 20. Unless otherwise stated, errors shown in tables and figures refer to 90% and 1 σ errors, respectively.

3 DATA ANALYSIS

We first examine how the broadband spectrum of Mrk 1018 varies over time. Figure 1 shows the spectra from optical to X-ray in 2008 Jun (red) and Aug (black), 2013 (green), and 2016 (blue). It is clear that there is considerable difference in the variability across the spectrum. The optical remains

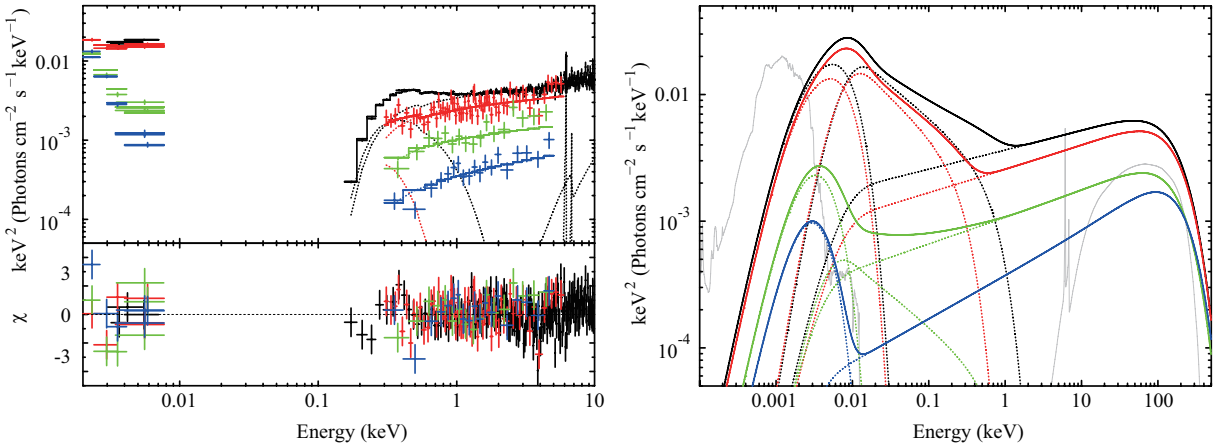

Figure 1. Left: Optical, UV, and X-ray spectra in 2008 Aug (black), 2008 Jun (red), 2013 (green), and 2016 (blue) in νF_ν forms, fitted with the model of `phabs*redden*(optxagnf + MYTorusS + MYTorusL + hostpol)`. Right: Best-fit AGN model spectra shown after the absorption and reddening are removed, and in the same colors as in left panels. Grey shows model spectra of an S0-type host galaxy emission, and a torus reflection component accompanied by fluorescence lines in 2008 Aug.

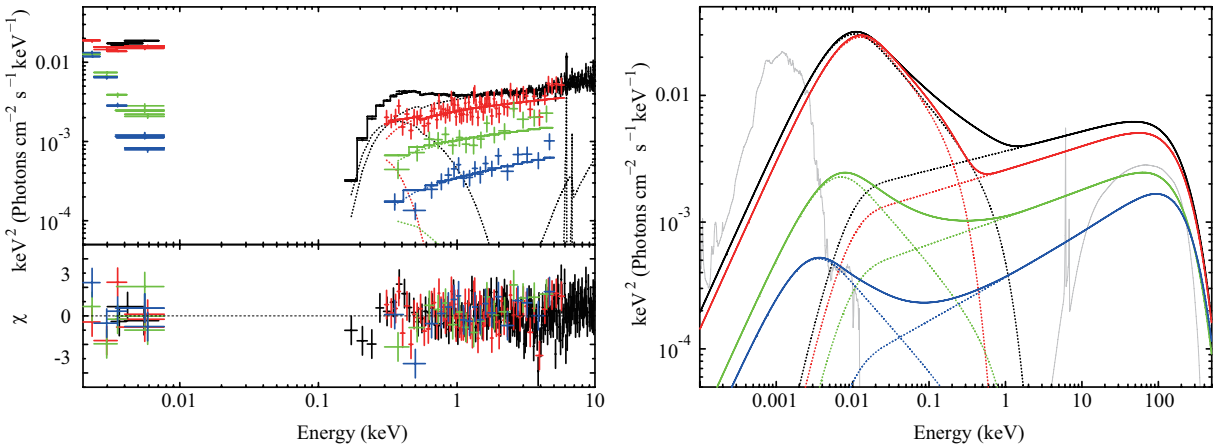

Figure 2. Same as Fig. 1, but with the model of `phabs*redden*(nthcomp_S + nthcomp_H + MYTorusS + MYTorusL + hostpol)`.

fairly constant, indicating a large contribution from the host galaxy, while the UV drops by over an order of magnitude. The X-rays also dim, but by a smaller factor, and change shape from that showing a strong soft X-ray excess below 1 keV in the brightest spectrum (2008 Aug: black) which disappears in the dimmer spectra.

3.1 Outer disc, soft Comptonization, hard Comptonization model

To quantify the spectral shape variations in optical, UV and X-ray, we first perform the broadband AGN spectral fit with a standard SMBH accretion model containing the disc emission, the soft X-ray excess, and the hard Comptonization continuum `optxagnf` (Done et al. 2012), modified by the Galactic photo-absorption and reddening effects modeled by `phabs` and `redden`, respectively. This assumes a standard disc emissivity (Novikov-Thorne), but that this energy is only dissipated in a standard disc structure from the outer radius $R_{\rm out}$ to a coronal radius $R_{\rm cor}$ which is a free parameter. Within $R_{\rm cor}$, the gravitational energy is split, with a fraction $f_{\rm PL}$ powering the coronal X-ray power-law emission, characterized by a photon index $\Gamma_{\rm H}$, and the remainder dissipated in a warm Comptonization component, characterized by electron temperature $kT_{\rm e}$ and optical depth τ. This model has enough flexibility to fit to AGN spectra, but with the physical constraint that all the emission is assumed to be powered by a constant mass accretion rate, parameterized as $L/L_{\rm Edd}$ for a given SMBH mass $M_{\rm BH}$ and spin a^*. This additional energy conservation assumption allows the model components to be constrained across the unobservable EUV region. The model then is normalized by the physical parameters of $M_{\rm BH}$, $L/L_{\rm Edd}$, a^* and co-moving distance D. Mrk 1018 has single epoch black hole mass of $\log(M_{\rm BH}/M_\odot) = 7.4$–$7.9$ (McElroy et al. 2016). We use $\log(M_{\rm BH}/M_\odot) = 7.84$ in all that follows Ezhikode et al. (2017), and assume $a^* = 0$ following previous SED fits to the 2008 data with `optxagnf`. We use the co-moving distance of $D \sim 176$ Mpc, corresponding to the source redshift of $z = 0.042$.

The X-ray data also show a clear Fe-Kα at ~ 6.4 keV in the *XMM-Newton* spectrum of 2008 Aug. The remaining *Swift* datasets have insufficient signal-to-noise to constrain this feature, but comparison of a *Chandra* observations from 2010 and 2016 (not included here as these have no simultane-

Table 1. Model parameters obtained by the fits to the optical, UV and X-ray spectra in 2008 Aug, 2008 Jun, 2013, and 2016.

Component	Parameter	2008 Aug	2008 Jun	2013	2016
`phabs`	$N_{\rm H}$ (10^{20} cm^{-2})		2.43 (fix)		
`redden`	$E(B-V)$		$=1.5\times N_{\rm H}/(10^{22}$ cm$^{-2})$		
			Fit with outer standard disc		
`optxagnf`	$M_{\rm BH}$ ($M_\odot$)		6.92×10^7 (fix)		
	D (Mpc)		176 (fix)		
	$\log(L/L_{\rm Edd})$	$-1.14^{+0.02}_{-0.03}$	$-1.26^{+0.04}_{-0.08}$	$-1.93^{+0.07}_{-0.06}$	-2.27 ± 0.03
	a^*		0 (fix)		
	$R_{\rm cor}$ ($R_{\rm g}$)		$60.0^{+71.8}_{-24.3}$	$73.7^{+52.0}_{-5.3}$	
	$R_{\rm out}$ ($R_{\rm g}$)		$=$ Self gravity radius $=2.3\times10^3(L/L_{\rm Edd})^{4/9}$		
	$kT_{\rm e}$ (keV)	0.17 ± 0.02	$0.07^{+0.07}_{-0.02}$	$=kT_{\rm e}$ in 2008 Aug	
	τ	$18.5^{+1.6}_{-1.2}$	$29.3^{+37.9}_{-27.3}$	$=\tau$ in 2008 Aug	
	$\Gamma_{\rm H}$	1.85 ± 0.03	$1.82^{+0.07}_{-0.09}$	$1.79^{+0.10}_{-0.09}$	1.66 (fix)
	$f_{\rm PL}=L_{\rm H}/(L_{\rm S}+L_{\rm H})$	$0.48^{+0.22}_{-0.05}$	$0.47^{+0.10}_{-0.08}$	$0.91^{+0.06}_{-0.11}$	0.85–1
	z		0.0424 (fix)		
	N		1 (fix)		
χ^2/d.o.f.			326.5/267		
			Fit without outer standard disc		
`nthcomp_S`	$\Gamma_{\rm S}$		$2.68^{+0.15}_{-0.09}$		
	$kT_{\rm e,S}$ (keV)	$0.20^{+0.05}_{-0.02}$	$0.06^{+0.02}_{-0.01}$	$=kT_{\rm e,S}$ in 2008 Aug	
	$kT_{\rm bb,S}$ (eV)	$3.01^{+0.54}_{-0.42}$	$3.62^{+1.10}_{-0.66}$	$1.99^{+1.00}_{-0.56}$	$1.00^{+0.61}_{-0.00b}$
	z		0.042436 (fix)		
	$N_{\rm S}$ (10^{-5})	$48.11^{+10.29}_{-8.22}$	$(2.09^{+4.12}_{-0.98})\times10^{-2}$	$2.71^{+1.63}_{-0.92}$	$0.39^{+0.21}_{-0.10}$
	$L_{\rm S}$ (10^{44} erg/s)	6.30 ± 0.16	$5.56^{+0.20}_{-0.19}$	0.48 ± 0.04	0.11 ± 0.02
`nthcomp_H`	$\Gamma_{\rm H}$	1.85 (fix)	1.82 (fix)	1.79 (fix)	1.66 (fix)
	$kT_{\rm e,H}$ (keV)		100		
	$kT_{\rm bb,H}$ (eV)		$=kT_{\rm bb,S}$		
	z		0.042436 (fix)		
	$N_{\rm H}$ (10^{-3})	3.63 ± 0.05	$2.60^{+0.11}_{-0.12}$	1.09 ± 0.11	0.37 ± 0.03
	$L_{\rm H}$ (10^{44} erg/s)	2.71 ± 0.03	2.04 ± 0.09	0.91 ± 0.09	0.45 ± 0.04
χ^2/d.o.f.			314.2/269		

ous optical/UV data) shows that the line is narrow, and neutral, consistent with an origin in the torus (LaMassa et al. 2017). Hence, from physically-motivated torus reflection models called `MYTorus`, we include a Compton-scattered component and emission lines (hereafter we call `MYTorusS` and `MYTorusL` respectively), calculated with a Comptonized thermal intrinsic continuum with the electron temperature of 100 keV. We fix the optical depth for the intrinsic continuum, inclination angle, and the redshift at 0.8, 0°, and 0.0424, respectively, while the column density of the torus and the normalization are tied between `MYTorusS` and `MYTorusL`, and left free. In 2008 Jun, 2013, and 2016, the torus reflection cannot be well constrained due to the usable energy range (see §2), we set the normalizations in `MYTorusS` and `MYTorusE` to zero.

The optical data clearly also show a constant host galaxy component. This is a late type merger, categorized as a lenticular galaxy (the S0 type in the Hubble classification, e.g. Winter et al. 2010). Following Ezhikode et al. (2017), we add a model of S0-type host galaxy emission template named `hostpol` (Polletta et al. 2007). We tie the normalization of `hostpol` across the four spectra. The total model fit to the four datasets simultaneously is then `phabs*redden*(optxagnf + MYTorusS + MYTorusL + hostpol)`. The column density $N_{\rm H}$ of `phabs` is fixed at the Galactic value of 2.43×10^{22} cm^{-2}, while $E(B-V)$ of `redden` is tied to $1.5\times N_{\rm H}/(10^{22}$ cm$^{-2})$ utilizing the Galactic gas-dust ratio. The *Swift* data especially cannot constrain all the parameters of the `optxagnf` model. We tie the coronal outer radius $R_{\rm cor}$ between 2008 Jun and Aug, and between 2013 and 2016. In addition, we fix $\Gamma_{\rm H}$ in 2016 at 1.66 following the 2016 phenomenological fit result without the `MYTorus` models in LaMassa et al. (2017), considering that the normalizations of the `MYTorus` models are fixed at zero.

We first fit the four spectra by making the electron temperature $kT_{\rm e}$ and optical depth τ of the soft Comptonization in `optxagnf` free and tied among all. In the fit, the systematic errors of 3% are employed to account for the calibration uncertainties mainly in absolute flux scaling between the OM and UVOT (e.g., Lobban et al. 2016). The fit is not acceptable, with χ^2/d.o.f.$=347.5/269$, mainly because of large negative residuals in the soft X-ray band in 2008 Jun, showing that the soft X-ray excess spectral shape is different between 2008 Jun and Aug. Allowing $kT_{\rm e}$ and τ in 2008 Jun to differ from those in 2008 Aug gives an almost acceptable fit with χ^2/d.o.f.$=326.5/267$. Figure 1 left shows

the data fit to this model, together with the residuals, while Fig. 1 right shows the unabsorbed model components. The best fit parameter values and 90% confidence uncertainties are given in Table 1.

3.2 No outer disc model

Recently, the optical/UV emission from an AGN has been interpreted by only a soft X-ray excess component without an outer standard disc (e.g., Mehdipour et al. 2015; Petrucci et al. 2017). However, there is still implicitly an outer disc as the model requires that there is some source of seed photons for the warm Comptonization. Petrucci et al. (2017) assume that these seed photons have a disc blackbody distribution, and this is a key to their optical/UV slope being able to fit many of their objects. The maximum seed photon temperature of the disc blackbody, $kT_{\rm bb,S}$, is left as a free parameter. This contrasts with the `optxagnf` model where the original picture was that the seed photons came from the disc underlying the warm Comptonization region (see Appendix A in Done et al. 2012), but since these would affect the spectrum only in the unobservable EUV regime the code approximated these by blackbody seed photons at the temperature of the hottest part of the standard disc i.e. $T(R_{\rm cor})$. Thus we try the Petrucci et al. (2017) model of `phabs*redden*(nthcomp_S + nthcomp_H + MYTorusS + MYTorusL + hostpol)`. The warm Comptonization is modeled by `nthcomp_S`, while `nthcomp_H` models the coronal power-law emission, and both are assumed to have the same seed photon distribution, characterized by a disc blackbody with maximum temperature $kT_{\rm bb,S}$.

Similarly to the `optxagnf` fits above, the data strongly require that the soft X-ray excess shape in 2008 Jun is different from 2008 Aug. Hence if we tie the photon index of the warm Comptonization between the four spectra then the data strongly require that its electron temperature is different. Conversely, if we tie the electron temperature then we require that the photon index of the warm Comptonization changes. We choose then to tie the warm Comptonization spectral index $\Gamma_{\rm S}$ between the four spectra, as Petrucci et al. (2017) give some physical reasons for fixing this from reprocessing of the warm Comptonization in a passive, optically thick disc beneath the corona. Because the warm Comptonization component is not significantly detected in the soft X-ray emission in 2013 and 2016, we tie the `nthcomp_S` coronal temperature $kT_{\rm e,S}$ across all the 2008 Jun, 2013, and 2016 datasets. We allow the seed photon temperature to be free in all datasets. The coronal Comptonization seed photon temperature is set to that of the soft Comptonization in all datasets, but it is assumed to be blackbody rather than disc blackbody. The photon index $\Gamma_{\rm H}$ is fixed at those obtained by the fit with `optxagnf` to compare the reproducibility of the optical–UV band between the two models, and we fix the `nthcomp_H` coronal temperature $kT_{\rm e,H} = 100$ keV as in `optxagnf`. Reflection, host galaxy and absorption are included as before.

This somewhat different spectral decomposition gives a similarly good fit with χ^2/d.o.f.$= 314.2/269$ (see table 1), showing that the optical can be modeled either by assuming an outer standard disc or by assuming that there is optically thick material which reprocesses the emission from a warm Comptonizing layer above it. The best fit model is shown against the data in Fig. 2 left and as unabsorbed model components in Fig. 2 right.

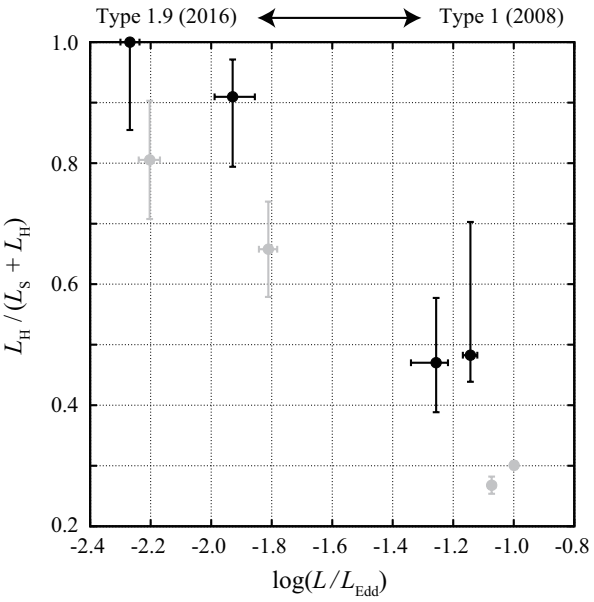

Figure 3. The $L/L_{\rm Edd}$-dependence of the fraction of the soft and hard Comptonization strengths written as $L_{\rm S}$ and $L_{\rm H}$ respectively. These are obtained by the spectral fits with `optxagnf` (black) and `nthcomp_S` + `nthcomp_H` (grey) summarized in Fig. 1, Fig. 2, and Table 1. Errors here refer to 90% errors.

3.3 Changing broadband continuum spectral shape

These models are both acceptable fits to the data, and allow us to characterize how the accretion flow emission changes as a function of $L/L_{\rm Edd}$. This is a direct parameter of the `optxagnf` modeling, but is not explicitly included in the warm and hot Comptonization description. Instead, we integrate the model components to get the luminosity in the warm and hard X-ray Comptonizing regions. This allows us to calculate $L/L_{\rm Edd}$ using the same mass and distance as before.

Both models have hard and soft Comptonization components, so Fig. 3 shows the change of $L_{\rm H}/(L_{\rm S}+L_{\rm H})$, which is equivalent to $f_{\rm PL}$, when we use `optxagnf` (black) and the two Comptonization components with no outer disc (grey). Both models show similar behaviour in that the warm and hot Comptonization components show comparable luminosity at $L/L_{\rm Edd} \sim 0.08$, but that the ratio of the hot component gets larger when $L/L_{\rm Edd}$ becomes smaller, and it dominates the spectrum at $L/L_{\rm Edd} \sim 0.006$. Note that the errors in the case of the two Comptonization components are relatively small mainly because the spectral shapes are fixed.

3.4 Summary of results

(i) The observed 2–10 keV flux drops by a factor of 6–7 over ~ 8 years, while the UV luminosity drops by a factor of ~ 20.

(ii) Broadband spectral models show that the total luminosity drops by a factor of 13–15, from $L/L_{\rm Edd} \sim 0.08$ to ~ 0.006.

(iii) The warm Comptonization region (soft X-ray excess) is very obvious when the source is brightest, where the broadband SED looks like a typical Seyfert type 1.

(iv) The warm Comptonization region may disappear completely as the source dims if there is residual emission from an outer standard disc (`optxagnf` model). Alternatively, the faint optical/UV emission may be produced entirely by the warm Comptonization, and not require any outer standard disc, in which case the warm Comptonization drops by a factor of ~ 60.

Previous models of these data assumed a simple disc and power law model for the optical/UV and X-ray flux, respectively, and did not specifically fit to the soft X-ray excess (Husemann et al. 2016). This is important as Fig. 1 and 2 show that almost all of the EUV photons, the ones which most contribute to the BLR ionization, are in the soft excess emission. Therefore, the changing-look phenomenon in Mrk 1018 from type 1.9 to 1 around 1980 (Cohen et al. 1986) and from type 1 to 1.9 around 2010 (McElroy et al. 2016) is clearly controlled by the increase and decrease of the warm Comptonization region, respectively. We will explicitly explore the effect of this changing spectral shape as well as luminosity on the predicted BLR emission from an LOC model in a following paper.

The soft X-ray excess probably forms the seed photons for the hot Comptonization component, so a decrease in the ratio between soft and hard Comptonization means a decrease in seed photons for Compton cooling of the hard X-ray emitting electrons relative to the power injected into heating these electrons (e.g., Beloborodov 1999). Hence, the large decrease of the warm Comptonization flux is likely to lead to spectral hardening of the hot Comptonization continuum, although significant photon index decrease of the hot Comptonization component is not supported by the data. This can be tested by longer X-ray observations especially of faint epochs in the future.

However, the remaining results are much more difficult to explain, as discussed below.

4 DISCUSSION

4.1 Standard accretion disc timescales

Fundamentally, we see a drop in total accretion luminosity by a factor of 13–15 over a timescale of ~ 8 years. This is a problem for any standard disc model. There is a hierarchy of timescales for a standard thin disc, with the dynamical timescale being fastest, then the thermal timescale and then the viscous. We calculate these for Mrk 1018, assuming that the optical/UV (typical temperature 3×10^4 K) is emitted from a standard thin disc at $R\sim100\,R_{\rm g}$. This implies $H/R = c_s/v_\phi \sim 5\times10^{-4}$ (where the sound speed $c_s=\sqrt{kT/m_p}$ and Keplarian velocity $v_\phi=\sqrt{GM/R}=\sqrt{R_{\rm g}/R}c$). The optical emission regions in AGN discs are much thinner than the optical parts of cataclysmic variables (CV) or BHB discs, as in AGN the optical is produced at $\sim 100\ R_{\rm g}$ rather than $10^5\ R_{\rm g}$ so while the gas temperature is the same for the optical emission, the Keplarian velocity on the denominator is much higher. For $\alpha=0.1$ these give expected timescales of

$$t_{\rm dy} \approx \left(\frac{GM_{\rm BH}}{R^3}\right)^{-\frac{1}{2}} \approx 4 \text{ days} \quad (1)$$

$$t_{\rm th} \approx \frac{t_{\rm dyn}}{\alpha} \approx 1 \text{ month} \quad (2)$$

$$t_{\rm vis} \approx \frac{t_{\rm dyn}}{\alpha}\left(\frac{H}{R}\right)^{-2} \approx 4\times10^5 \text{ years.} \quad (3)$$

The observed timescale of ~ 8 years is much shorter than the viscous timescale, while somewhat longer than the thermal and dynamical timescales. The thermal timescale in particular is suggested as the origin of the 10–20% stochastic optical variability which is typically seen in AGNs on timescales of months (e.g., Kelly et al. 2009; MacLeod et al. 2010). The magnetorotational instability (MRI) (Balbus & Hawley 1991) produces fluctuations in dissipation, leading to changes in local heating on a thermal timescale (e.g., Dexter & Agol 2011).

However, this stochastic variability on timescales of months is very different to the factor of at least ~ 20 systematic decrease in optical/UV over a period of ~ 8 years seen here. The amplitude of bolometric change requires that there is a change in either mass accretion rate or efficiency (or both) of the accretion flow, yet this change occurs on a timescale which is too fast for the mass accretion rate to change through a standard disc (viscous timescale) by many orders of magnitude.

4.2 Disc instability in BHBs

Variability in BHBs is much easier to study directly as the timescales are much shorter, of order days-months-years. There is now a good general understanding that their transient outbursts, where the mass accretion rate increases by orders of magnitude from quiescence to outburst, are triggered by the Hydrogen ionization (H-ionization) disc instability mechanism (DIM) in the outer disc. Mass accreting from the companion star accumulates at the circularization radius. This is initially cold, below the H-ionization point, so there are no free electrons and the opacity is low. The mass accretion rate through this structure is lower than the rate at which mass is added from the companion star so the surface density and temperature build up together until it reaches a temperature of ~ 3000 K, at which point part of the blackbody flux can start to ionize Hydrogen. This traps these photons in the material, so its temperature rises, which means more photons can ionize Hydrogen. This continues until all of the Hydrogen is ionized, i.e to a temperature of 10^4 K. This jump in temperature also gives a jump in sound speed, so matter can be transported through the disc faster i.e., the local accretion rate can now be larger. This can trigger the next ring inwards to go unstable to H-ionization, turning the local instability into a global switch in disc properties if the difference in mass accretion rate is large enough. This requires a change in the effective viscosity, often parameterized as a jump in α from neutral to ionized, perhaps as an outcome of the MRI either requiring free electrons (Menou et al. 1999) or driving turbulence (Coleman et al. 2016). This results in a heating front propagating inwards, traveling at a speed which is shorter than the

viscous timescale by a factor (H/R) (Hameury et al. 1998; Dubus et al. 2001; Lasota 2001; Hameury et al. 2009).

The mass accretion rate through the disc is now larger than the mass accretion rate from the companion star, so it cannot maintain this steady state structure. When the outer disc temperature falls below 10^4 K, the instability works in reverse, triggering a cooling wave through the disc which switches Hydrogen back to neutral and propagates at a speed faster than the heating front by a factor α_h/α_c.

In accreting white dwarf systems, the cooling wave is triggered quite quickly after the heating wave, shutting off the outburst after only a small amount of the total disc material is accreted (Osaki 1996). Instead, in BHBs and neutron stars, the copious X-ray emission from the inner disc which is associated with the much larger gravitational potential irradiates the outer disc material, keeping it ionized. The disc material accretes viscously (exponential decline) until the X-ray luminosity drops enough for the outer disc to dip below the H-ionization temperature. The cooling front starts, but its inward speed is set instead by the viscous shrinking of the irradiated zone, giving a linear decline (King & Ritter 1998).

Thus the mass accretion rate onto the black hole can increase by many orders of magnitude on timescales of days for the heating front propagation (Dubus et al. 2001), while the decline is rather slow as it is controlled by the viscous time of the outer disc. This mechanism is well tested in BHBs and neutron stars (Shahbaz et al. 1999; Coriat et al. 2012), and in white dwarfs (Osaki 1996).

4.3 State change in BHBs

The dramatic variability associated with the H-ionization DIM can also trigger a spectral transition, which most probably represents a switch in the nature of the accretion flow from a hot, optically thin, geometrically thick flow (low/hard, Comptonization dominated e.g. the advection dominated accretion flow: Narayan & Yi 1995) to a cool, optically thick, geometrically thin disc (high/soft, thermal dominated). This transition can occur over a wide range in luminosity on the fast rise to outburst, but this may be due to the flow being far from steady state (Smith et al. 2002; Gladstone et al. 2007). Instead, the reverse transition on the slow decline occurs at a rather stable luminosity around $0.02\,L_{\rm Edd}$ (Maccarone 2003, see e.g. the review by Done et al. 2007).

Cygnus X-1 shows this spectral transition decoupled from the DIM as its outer disc is stable. This shows that the hard state is on average a factor of ~ 3–4 lower in bolometric luminosity than the soft state (Zdziarski et al. 2002). This could be entirely produced by the state change alone, with a constant mass accretion rate as the hard state should be somewhat radiatively inefficient, and some of the accretion energy is required to power the potentially substantial kinetic luminosity of the compact jet seen in the radio emission (Zdziarski et al. 2002). However, some change in mass accretion rate is required to trigger the state change, so it seems more reasonable to assume that there are long timescale fluctuations in mass accretion rate of perhaps a factor of ~ 1.5–2 so that the bolometric luminosity at a single transition only changes by a factor ~ 1.5–2. Thus a state change can give a drop in luminosity by a factor 2–4 *without* requiring any change in mass accretion rate.

The soft to hard transition involves a quite dramatic decrease in surface density and concomitant increase in temperature (see e.g. the review by Yuan & Narayan 2014 Fig. 3). Changing the surface density radially requires a viscous timescale but here the disc evaporates so it can lose mass vertically as it heats up to the virial temperature. Shaviv & Wehrse (1986) show that even a standard Shakura-Sunyaev disc will have a thermal instability in its outer layers, as by definition the photosphere is rather inefficient at cooling, so any heat dissipated here heats up this material to the virial temperature. The next layer of the disc is then the photosphere, so it too heats up, and this process can lead to the entire disc switching into the hot solution (see e.g. Das & Sharma 2013; Hogg & Reynolds 2017). However, while this does involve vertical rather than radial motion, the timescales are still the radial viscous timescale (Czerny 2006) as can be seen most clearly from the reverse process of condensation at the soft-to-hard transition. The hot flow collapses down into the midplane, but its surface density is so much smaller than that of a standard disc that it requires a viscous timescale for radial accretion from the outer disc to build up the material back into a standard disc. Indeed, this is seen in BHBs, where the timescale for the soft-to-hard state transition is ~ 0.5 days which is close to the thin disc viscous timescale at a few hundreds R_g which is the expected radius of the evaporated region (Mayer & Pringle 2007).

4.4 Differences between AGNs and BHBs

Fundamentally, the behaviour of Mrk 1018 looks like a large drop in luminosity, similar to that seen in the transient BHBs which are triggered by the DIM, together with a state change as the luminosity drops below a few percent of Eddington. However, as has often been noted, the timescales predicted by the thin disc models or by scaling from galactic binaries are far too long. Here we critically assess these timescales, pointing out some significant differences between AGNs and BHBs.

A key difference between AGNs and BHBs is that the disc in AGNs is self-gravitating at around a few hundreds R_g (e.g., Laor & Netzer 1989). This outer disc radius is much smaller than the disc in BHBs, which is truncated by tidal effects from the companion star at typical radii of $R \sim 10^5\ R_g$. The combined effect of mass and radius predicts all timescales scale as $M r_{\rm out}^{3/2}$ where $R_{\rm out} = r_{\rm out} R_g$.

Another key difference, connected to the smaller $r_{\rm out}$ in AGNs, is in the importance of irradiation. This is effective only at large radii (Cunningham 1975; Shidatsu et al. 2016) so becomes mostly unimportant in AGN discs (Gardner & Done 2017). Thus the DIM in AGNs should be more comparable to the DIM in white dwarf systems, where irradiation is not important due to the much weaker white dwarf gravitational potential (Hameury et al. 2009). Thus the rise and decay times in AGNs should be set by the heating/cooling front propagation speeds, not by the viscous decay timescale.

We scale the DIM timescale from the observed dwarf novae ~ 1 day timescales of the heating/cooling front for a 1 $M_\odot$ white dwarf with $r_{\rm out} \sim 10^5$ up to an AGN with

mass $7 \times 10^7\ M_\odot$ and $r_{\rm out} \sim 10^2$. This predicts a timescale of ~ 6 years for the front propagation in AGNs, similar to that observed.

However, this assumed that H/R is similar in the AGN disc as in CV's, whereas a standard thin disc has $H/R = c_{\rm s}/v_\phi \sim (kT_{\rm gas}/m_{\rm p}c^2)^{1/2}(1/r_{\rm opt})^{1/2}$ which is much smaller in AGNs than in binaries (see §4.2 above). The front propagation timescale depends on R/H i.e. is a factor 30 longer than a simple scaling from CV's, lengthening the predicted timescale to ~ 1000 years. This is comparable to the timescales seen in the AGN DIM simulations of Hameury et al. (2009). Nonetheless, the data clearly show that the electron temperature in the soft X-ray excess region is two orders of magnitude higher than expected from the thin disc equations (0.2 keV rather than 2 eV). If this sets the scale height then AGN discs are more comparable in H/R to the CV discs, but it is very unclear how the DIM would then operate as the electron temperature is far above the H-ionization temperature required for the heating/cooling wave trigger.

There is one more break in the scaling between AGN and binaries, which is the importance of radiation pressure. The lower densities typical of AGN discs mean that gas pressure is lower at the same temperature, so radiation pressure is more likely to dominate. Thus the sound speed is set by the radiation pressure rather than the gas pressure, and is faster than in gas pressure dominated discs. For Mrk 1018 at its peak luminosity, radiation pressure is a factor ~ 75 larger than the gas pressure in the optical emission region (e.g., Laor & Netzer 1989). Radiation pressure was not included in the AGN DIM simulations of Hameury et al. (2009) as radiation pressure dominated discs are unstable (Shakura & Sunyaev 1973). This radiation pressure thermal-viscous instability is seen in all simulations where heating scales with total (gas plus radiation) pressure (e.g., Szuszkiewicz & Miller 2001), resulting in characteristic limit cycles between a slim, super-Eddington inner disc and a much dimmer standard disc at all luminosities $L > 0.05\ L_{\rm Edd}$. These are not typically observed in BHBs in this luminosity range (e.g., Gierliński & Done 2004), which could indicate that they are stabilized by magnetic pressure (e.g. Czerny et al. 2003; Grzędzielski et al. 2017). The total pressure should be even larger than that predicted by the radiation pressure dominated disc, giving an even faster sound speed for the heating/cooling front, though we note that current MRI simulations do not show magnetic pressure dominating as they show the instability (Jiang et al. 2013).

The large drop in luminosity could then be the DIM cooling front, propagating through a radiation and/or magnetic pressure dominated AGN disc. As the luminosity drops below a few percent of Eddington, it triggers the state transition as seen in BHBs. This occurs at more or less constant luminosity, but still requires a viscous timescale to change the surface density by evaporation/condensation. Scaling the BHBs soft to hard transition timescale of ~ 0.5 days by the mass difference alone (as both only affect the inner $100\ R_{\rm g}$ gives $\sim 10^4$ years, but this does not take into account the difference in H/R between the two systems, making the predicted timescale even longer. Again, this can be solved if the disc is dominated by radiation and/or magnetic pressure instead of gas pressure. Once the system has made the transition to a hot accretion flow it should vary on the viscous timescale of the hot flow, which is of order the thermal timescale as H/R is of order unity.

4.5 Observational predictions

As we suggest in §4.4, Mrk 1018 likely experiences both drop in mass accretion rate due to the cooling front propagation and spectral state transition by disc evaporation. Considering these processes individually, extremely variable AGNs are divided into three groups; (1) sources showing a state change due to disc evaporation/condensation associated with a factor 2–4 decrease/increase in luminosity, (2) sources with large mass accretion rate change due to the thermal front propagation due to the H-ionization instability, and (3) sources showing both.

We suggest that many of changing-look AGNs are included in the group (1) or (3), and their variations commonly cross the state transition boundary of $L/L \sim$ a few percent. Sources with the variability amplitude of a factor a few are probably categorized into group (1), while those with amplitude of factor more than 10 should be into group (3). Interestingly, many of the known changing-look AGNs, e.g., NGC 2617 (Shappee et al. 2014), Mrk 590 (Denney et al. 2014), and SDSS J0519+0033 (LaMassa et al. 2015) actually show $L/L_{\rm Edd} \sim$ a few percent. A similar drop in the soft X-ray excess is seen by Rivers et al. (2012) in Mrk 590 between 2004 and 2011, which we suggest is due to a state change associated with the changing-look phenomena, as in Mrk 1018. Recently, several tens changing-look AGNs have been newly reported (MacLeod et al. 2016; Yang et al. 2017), but their Eddington ratios have not been reported yet. We thus predict that these new changing-look AGNs have $L/L_{\rm Edd} \sim$ a few percent as well. Vice versa, we also predict that AGNs which exhibit drastic $L/L_{\rm Edd}$ variation crossing a few percent, e.g., NGC 3227 (Noda et al. 2014) and NGC 3516 (Noda et al. 2013) will experience changing-look phenomena simultaneously to drastic soft excess variation at $L/L_{\rm Edd} \sim$ a few percent. We need further continuous optical spectroscopic monitoring spontaneously to soft X-ray monitoring on these sources for unconfirmed changing-look phenomena.

As MacLeod et al. (2010) reported, quasar variability cannot be explained by stochastic optical fluctuations driven by accretion rate, and there is additional variability depending on black hole mass and/or luminosity. If the thermal front propagation occurs as group (2), variability amplitude is determined by swept disc area which varies with black hole mass, i.e., luminosity with fixed accretion rate. Thus, the quasar variability may include that by the front propagation through a thin disc (e.g., Hameury et al. 2009), and some quasars are perhaps included into group (2) although they do not show the changing-look features. This can be tested by investigating detailed radial profile of disc temperature in quasars, which might include discontinuous drop if a thermal front is present. If their $L/L_{\rm Edd}$ could cross a few percent by the front propagation like Mrk 1018, they would show state transition, and enter group (3) being a changing-look quasar as reported by (LaMassa et al. 2015).

5 CONCLUSIONS

In the present paper, we show for the first time how the changing-look phenomenon is linked to a large change in the warm Comptonization component which forms the soft X-ray excess. The bolometric luminosity drops from $\sim 0.08\,L_{\rm Edd}$ to $\sim 0.006\,L_{\rm Edd}$, but the hard X-rays drop by only a factor ~ 7 while the warm Comptonization decreases by at least a factor ~ 60 and may disappear completely. This marked hardening of the spectrum looks very like the transition seen in stellar mass BHBs around $0.02\,L_{\rm Edd}$, which is generally interpreted as the inner regions of an optically thick accretion disc evaporating into a hot accretion flow. We suggest that all the true changing-look AGNs make this spectral transition to/from an EUV bright accretion disc to a hot inner flow, and that the change in BLR properties is a mostly a consequence of the changing shape of the ionizing spectrum.

While the state transition describes the changing shape of the spectrum, the timescale for disc evaporation/condensation should be the viscous timescale of the disc. This predicts far too long a timescale compared to that observed. There is a similar problem in explaining the background decline in flux which triggers the transition. In Mrk 1018 the optical flux drops by more than a factor of 10, requiring a true change in mass accretion rate over a timescale of ~ 10 years, orders of magnitude shorter than the viscous timescale. We discuss all the factors which change between AGN and binary discs so as to properly scale between them, as sizes and scale heights should be different. However, one key difference which has not been considered so far is that AGN discs are dominated by radiation pressure even in standard disc models. Thus the sound speed, and hence the viscous speed, is much faster for a given gas temperature. Including magnetic pressure to stabilize the disc again increases the sound speed, making it feasible that there can be correspondence between the observations and theory. We suggest the Hydrogen ionization disc instability, where the heating/cooling front travels on a speed which is faster than the viscous timescale by a factor H/R, as the underlying mechanism for the flux drop. We speculate that this is the origin of the most extreme AGN variability. Proper modeling of this is required in order to predict the behaviour in more detail.

ACKNOWLEDGEMENTS

We thank the referee for his/her careful read of this manuscript and valuable comments. HN is supported by Program for Establishing a Consortium for the Development of Human Resources in Science and Technology, Japan Science and Technology Agency (JST). CD acknowledges the Science and Technology Facilities Council (STFC) through grant ST/P000541/1 for support. This work made use of data supplied by the UK Swift Science Data Centre at the University of Leicester.

REFERENCES

Balbus, S. A., & Hawley, J. F. 1991, ApJ, 376, 214
Beloborodov, A. M. 1999, High Energy Processes in Accreting Black Holes, 161, 295
Baldwin, J., Ferland, G., Korista, K., & Verner, D. 1995, ApJ, 455, L119
Begelman, M. C., & Pringle, J. E. 2007, MNRAS, 375, 1070
Clavel, J., Nandra, K., Makino, F., et al. 1992, ApJ, 393, 113
Cohen, R. D., Puetter, R. C., Rudy, R. J., Ake, T. B., & Foltz, C. B. 1986, ApJ, 311, 135
Coleman, M. S. B., Kotko, I., Blaes, O., Lasota, J.-P., & Hirose, S. 2016, MNRAS, 462, 3710
Coriat, M., Fender, R. P., & Dubus, G. 2012, MNRAS, 424, 1991
Cunningham, C. T. 1975, ApJ, 202, 788
Czerny, B., Nikołajuk, M., Różańska, A., et al. 2003, A&A, 412, 317
Czerny, B. 2006, Astronomical Society of the Pacific Conference Series, 360, 265
Das, U., & Sharma, P. 2013, MNRAS, 435, 2431
Denney, K. D., De Rosa, G., Croxall, K., et al. 2014, ApJ, 796, 134
Dexter, J., & Agol, E. 2011, ApJ, 727, L24
Done, C., Gierliński, M., & Kubota, A. 2007, A&ARv, 15, 1
Done, C., Davis, S. W., Jin, C., Blaes, O., & Ward, M. 2012, MNRAS, 420, 1848
Dubus, G., Hameury, J.-M., & Lasota, J.-P. 2001, A&A, 373, 251
Dunn, R. J. H., Fender, R. P., Körding, E. G., Belloni, T., & Cabanac, C. 2010, MNRAS, 403, 61
Elitzur, M. 2012, ApJ, 747, L33
Elvis, M., Wilkes, B. J., McDowell, J. C., et al. 1994, ApJS, 95, 1
Evans, P. A., Beardmore, A. P., Page, K. L., et al. 2007, A&A, 469, 379
Evans, P. A., Beardmore, A. P., Page, K. L., et al. 2009, MNRAS, 397, 1177
Ezhikode, S. H., Gandhi, P., Done, C., et al. 2017, MNRAS, 472, 3492
Fragile, P. C., Etheridge, S. M., Anninos, P., Mishra, B., & Kluźniak, W. 2018, ApJ, 857, 1
Gierliński, M., & Done, C. 2004, MNRAS, 349, L7
Gardner, E., & Done, C. 2017, MNRAS, 470, 3591
Graham, M. J., Djorgovski, S. G., Drake, A. J., et al. 2017, MNRAS, 470, 4112
Grzędzielski, M., Janiuk, A., Czerny, B., & Wu, Q. 2017, A&A, 603, A110
Gezari, S., Hung, T., Cenko, S. B., et al. 2017, ApJ, 835, 144
Gladstone, J., Done, C., & Gierliński, M. 2007, MNRAS, 378, 13
Hameury, J.-M., Menou, K., Dubus, G., Lasota, J.-P., & Hure, J.-M. 1998, MNRAS, 298, 1048
Hameury, J.-M., Viallet, M., & Lasota, J.-P. 2009, A&A, 496, 413
Hirose, S., Blaes, O., & Krolik, J. H. 2009, ApJ, 704, 781
Hogg, J. D., & Reynolds, C. S. 2017, ApJ, 843, 80
Honma, F., Matsumoto, R., & Kato, S. 1991, PASJ, 43, 147
Husemann, B., Urrutia, T., Tremblay, G. R., et al. 2016, A&A, 593, L9
Jiang, Y.-F., Stone, J. M., & Davis, S. W. 2013, ApJ, 778, 65
Kelly, B. C., Bechtold, J., & Siemiginowska, A. 2009, ApJ, 698, 895-910
King, A. R., & Ritter, H. 1998, MNRAS, 293, L42
Korista, K., Baldwin, J., Ferland, G., & Verner, D. 1997, ApJS, 108, 401
Korista, K. T., & Goad, M. R. 2000, ApJ, 536, 284
LaMassa, S. M., Cales, S., Moran, E. C., et al. 2015, ApJ, 800, 144
LaMassa, S. M., Yaqoob, T., & Kilgard, R. 2017, ApJ, 840, 11
Laor, A., & Netzer, H. 1989, MNRAS, 238, 897
Lasota, J.-P. 2001, New Astron. Rev., 45, 449
Lawrence, A. 2012, MNRAS, 423, 451
Lawrence, A., Bruce, A. G., MacLeod, C., et al. 2016, MNRAS, 463, 296
Lobban, A. P., Vaughan, S., Pounds, K., & Reeves, J. N. 2016, MNRAS, 457, 38
Lusso, E., & Risaliti, G. 2016, ApJ, 819, 154

Maccarone, T. J. 2003, A&A, 409, 697
MacLeod, C. L., Ivezić, Ž., Kochanek, C. S., et al. 2010, ApJ, 721, 1014
MacLeod, C. L., Ross, N. P., Lawrence, A., et al. 2016, MNRAS, 457, 389
Matt, G., Marinucci, A., Guainazzi, M., et al. 2014, MNRAS, 439, 3016
Mayer, M., & Pringle, J. E. 2007, MNRAS, 376, 435
McElroy, R. E., Husemann, B., Croom, S. M., et al. 2016, A&A, 593, L8
Mehdipour, M., Branduardi-Raymont, G., Kaastra, J. S., et al. 2011, A&A, 534, A39
Mehdipour, M., Kaastra, J. S., Kriss, G. A., et al. 2015, A&A, 575, A22
Menou, K., Esin, A. A., Narayan, R., et al. 1999, ApJ, 520, 276
Narayan, R., & Yi, I. 1995, ApJ, 452, 710
Noda, H., Makishima, K., Yamada, S., et al. 2011, PASJ, 63, S925
Noda, H., Makishima, K., Nakazawa, K., et al. 2013, PASJ, 65, 4
Noda, H., Makishima, K., Nakazawa, K., & Yamada, S. 2013, ApJ, 771, 100
Noda, H., Makishima, K., Yamada, S., et al. 2014, ApJ, 794, 2
Noda, H., Minezaki, T., Watanabe, M., et al. 2016, ApJ, 828, 78
Oda, H., Machida, M., Nakamura, K. E., & Matsumoto, R. 2009, ApJ, 697, 16
Ohsuga, K., Mineshige, S., Mori, M., & Kato, Y. 2009, PASJ, 61, L7
Osaki, Y. 1996, PASP, 108, 39
Petrucci, P. O., Ursini, F., De Rosa, A., et al. 2017, arXiv:1710.04940
Polletta, M., Tajer, M., Maraschi, L., et al. 2007, ApJ, 663, 81
Porquet, D., Reeves, J. N., Matt, G., et al. 2018, A&A, 609, A42
Rivers, E., Markowitz, A., Duro, R., & Rothschild, R. 2012, ApJ, 759, 63
Sądowski, A. 2016, MNRAS, 459, 4397
Sakimoto, P. J., & Coroniti, F. V. 1981, ApJ, 247, 19
Shahbaz, T., van der Hooft, F., Casares, J., Charles, P. A., & van Paradijs, J. 1999, MNRAS, 306, 89
Shakura, N. I., & Sunyaev, R. A. 1973, A&A, 24, 337
Shappee, B. J., Prieto, J. L., Grupe, D., et al. 2014, ApJ, 788, 48
Shaviv, G., & Wehrse, R. 1986, A&A, 159, L5
Shidatsu, M., Done, C., & Ueda, Y. 2016, ApJ, 823, 159
Smith, D. M., Heindl, W. A., & Swank, J. H. 2002, ApJ, 569, 362
Szuszkiewicz, E., & Miller, J. C. 2001, MNRAS, 328, 36
Taam, R. E., & Lin, D. N. C. 1984, ApJ, 287, 761
Troyer, J., Starkey, D., Cackett, E. M., et al. 2016, MNRAS, 456, 4040
Winter, L. M., Lewis, K. T., Koss, M., et al. 2010, ApJ, 710, 503
Yang, Q., Wu, X.-B., Fan, X., et al. 2017, arXiv:1711.08122
Yuan, F., & Narayan, R. 2014, ARA&A, 52, 529
Zdziarski, A. A., Poutanen, J., Paciesas, W. S., & Wen, L. 2002, ApJ, 578, 357

This paper has been typeset from a TEX/LATEX file prepared by the author.